

Multistep Coulomb excitation of ^{64}Ni : Shape coexistence and nature of low-spin excitations

D. Little,^{1,2} A. D. Ayangeakaa ^{1,2,*} R. V. F. Janssens ^{1,2,†} S. Zhu,^{3,‡} Y. Tsunoda ^{4,5} T. Otsuka,^{6,7,8} B. A. Brown,^{9,10} M. P. Carpenter ¹¹ A. Gade,^{9,10} D. Rhodes,^{9,10,§} C. R. Hoffman,¹¹ F. G. Kondev ¹¹ T. Lauritsen,¹¹ D. Seweryniak,¹¹ J. Wu,¹¹ J. Henderson,¹² C. Y. Wu ¹² P. Chowdhury,¹³ P. C. Bender ¹³ A. M. Forney ^{14,¶} and W. B. Walters ¹⁴

¹*Department of Physics and Astronomy, University of North Carolina Chapel Hill, Chapel Hill, North Carolina 27599, USA*

²*Triangle Universities Nuclear Laboratory, Duke University, Durham, North Carolina 27708, USA*

³*National Nuclear Data Center, Brookhaven National Laboratory, Upton, New York 11973, USA*

⁴*Center for Computational Sciences, University of Tsukuba, 1-1-1 Tennodai, Tsukuba, Ibaraki 305-8577, Japan*

⁵*Center for Nuclear Study, The University of Tokyo, 7-3-1 Hongo, Bunkyo, Tokyo 113-0033, Japan*

⁶*Department of Physics, The University of Tokyo, 7-3-1 Hongo, Bunkyo, Tokyo 113-0033, Japan*

⁷*RIKEN Nishina Center, 2-1 Hirosawa, Wako, Saitama 351-0198, Japan*

⁸*KU Leuven, Instituut voor Kern- en Stralingsfysica, 3000 Leuven, Belgium*

⁹*National Superconducting Cyclotron Laboratory, Michigan State University, East Lansing, Michigan 48824, USA*

¹⁰*Department of Physics and Astronomy, Michigan State University, East Lansing, Michigan 48824, USA*

¹¹*Physics Division, Argonne National Laboratory, Argonne, Illinois 60439, USA*

¹²*Lawrence Livermore National Laboratory, Livermore, California 94550, USA*

¹³*Department of Physics, University of Massachusetts Lowell, Lowell, Massachusetts 01854, USA*

¹⁴*Department of Chemistry and Biochemistry, University of Maryland College Park, College Park, Maryland 20742, USA*



(Received 30 June 2022; accepted 28 September 2022; published 14 October 2022)

The structure of ^{64}Ni , the heaviest stable Ni isotope, has been investigated via high-statistics, multistep safe Coulomb excitation to search for shape coexistence, a phenomenon recently observed in neutron-rich ^{66}Ni and ^{70}Ni as well as in doubly magic, $N = 40$, ^{68}Ni . The study was motivated by recent, state-of-the-art Monte Carlo shell-model calculations (MCSM), where a Hamiltonian with effective interactions incorporating the monopole tensor force predicts the existence of shape coexistence, also in the lower-mass $^{62,64}\text{Ni}$ isotopes. A set of transition and static $E2$ matrix elements for both yrast and near-yrast structures was extracted from the differential Coulomb excitation cross sections. From comparisons between the new results and MCSM as well as other shell-model calculations, a clearer picture of the structure of ^{64}Ni emerges. Specifically, the low-spin states are shown to be dominated by proton and neutron excitations mainly within the fp shell, with minimal contribution from the $g_{9/2}$ shape-driving neutron orbital. The agreement between experimental data and MCSM results indicates a small oblate deformation for the 0_2^+ level and a spherical shape for the 0_3^+ state. In addition, the small upper limit determined for the $B(E2)$ probability of a transition associated with the decay of the recently observed 3463-keV, 0_4^+ state agrees with its proposed assignment to a prolate shape, herewith providing first evidence for triple shape coexistence in a stable Ni isotope.

DOI: [10.1103/PhysRevC.106.044313](https://doi.org/10.1103/PhysRevC.106.044313)

I. INTRODUCTION

At present, knowledge about the nickel isotopic chain extends from the proton dripline at ^{48}Ni [1] to the neutron-rich ^{78}Ni nucleus [2]. This semimagic ($Z = 28$) chain provides opportunities to document the evolution of nuclear structure as a function of neutron excess as it spans the neutron shell

closures at $N = 20$, 28, and 50 as well as a subshell closure at $N = 40$. By now, the nucleus ^{68}Ni has been shown to exhibit structural aspects consistent with a double-shell closure [3,4]. More recent interest in its structure has arisen, however, from the observation of triple shape coexistence [5,6]. Indeed, based on comparisons with the results of Monte Carlo shell-model (MCSM) calculations [5], the ground state has been associated with a spherical shape, the 1605-keV, 0_2^+ state with oblate deformation, and the 2511-keV, 0_3^+ level with a prolate one. The role of excitations associated with different shapes was subsequently emphasized further by the discovery of a 1567-keV, 0_2^+ state in ^{70}Ni [6,7]. This level is proposed to be associated with a prolate minimum, based on comparisons with the MCSM calculations, and is located roughly 1 MeV lower in excitation energy than the corresponding prolate 0_3^+ state in ^{68}Ni . Most recently, a similar

* ayangeak@unc.edu

† rvfj@email.unc.edu

‡ Deceased.

§ Present address: TRIUMF, 4004 Wesbrook Mall, Vancouver, Canada BC V6T 2A3.

¶ Present address: Sensors and Electromagnetic Applications Laboratory, Georgia Tech Research Institute, Atlanta, Georgia 30318.

situation has been discovered in ^{66}Ni , where the first four 0^+ states are now known [8,9]. The ground state and the 0_3^+ , 2671-keV level are understood as being associated with sphericity, while the 0_2^+ , 2443-keV and 0_4^+ , 2974-keV states are proposed to be located in oblate and prolate minima, respectively. Coexistence and transitions between spherical and deformed structures in this mass region can be understood in the context of so-called type-II shell evolution, as a consequence of the action of the monopole component of the proton-neutron tensor force between the $\pi f_{5/2,7/2}$ and the $\nu g_{9/2}$ orbitals [10–12]. Specifically, the occupation of the $\nu g_{9/2}$ orbital affects the $\pi(f_{7/2} - f_{5/2})$ gap, thereby facilitating pair excitations across the $Z = 28$ gap. An enhanced $\pi f_{5/2}$ occupation also reduces the energy of the $\nu g_{9/2}$ subshell, resulting in enhanced neutron particle-hole excitations across the $N = 40$ gap; i.e., multi particle-hole excitations induce changes in the effective single-particle energies and result in level sequences associated with different shapes. Generally speaking, it is worth noting that, as pointed out in Refs. [13,14], shape coexistence phenomena in the Ni, Sn, and Pb regions of the nuclear chart can all be viewed as resulting from multi particle-hole excitations.

Extensive experimental work has shown that the $N = 40$ neutron subshell gap is rather fragile and that deformed structures become yrast as protons are removed. This is the case, for example, with some of the neutron-rich Cr, Mn, Fe, and Co isotopes, where the level structures are dominated by deformed configurations and collective excitations involving the shape-driving $\nu g_{9/2}$ orbital [15–31]. In the Ni isotopic chain itself, signatures of collectivity have been reported in $^{62,63}\text{Ni}$ [32,33] through the presence of rotational bands at moderate and high spins ($I \geq 8$). Such bands have thus far not been observed in any heavier isotope: only high-spin sequences characteristic of particle-hole excitations have been observed in $^{64,66,67,68}\text{Ni}$ [34,35].

The present work focuses on ^{64}Ni with the objective to determine, with good precision via multistep Coulomb excitation, the transition probabilities to as many levels as possible near the ground state in order to provide information on their intrinsic structure in a model-independent manner and to compare the observations with the results of shell-model calculations carried out with the effective interactions used recently to describe the neutron-rich isotopes. In particular, it should be noted that MCSM calculations [5] predict that the presence of potential minima associated with spherical, oblate, and prolate shapes seen in the neutron-rich even Ni isotopes persists down to ^{64}Ni and ^{62}Ni . Two excited 0^+ levels have been observed earlier in ^{64}Ni at respective excitation energies of 2867 and 3026 keV [34]. The deexcitation of both states to the 2_1^+ level has been observed and $B(E2)$ transitions probabilities were obtained. Their values indicate that the two states are not associated with prolate deformation. Further, it will be shown that the calculations are able to reproduce the general feeding pattern exhibited by the Coulomb excitation data and provide an understanding for the absence of collective excitations.

Most recently, while the present work was nearing completion, evidence for the predicted shape coexistence in ^{64}Ni has

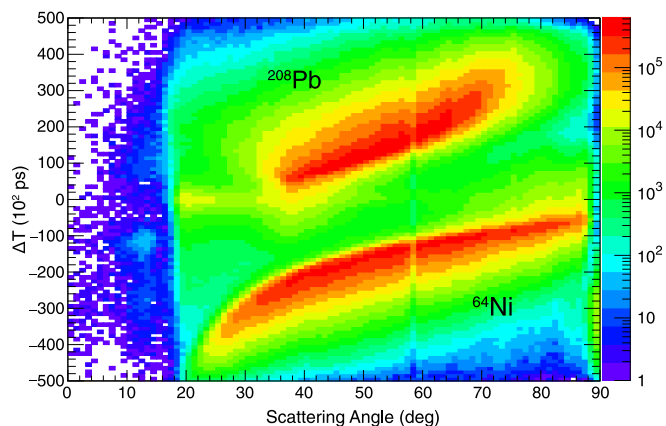


FIG. 1. Time-of-flight difference between the projectile and target recoils as a function of scattering angle measured with the CHICO2 detector. A clear separation between the ^{64}Ni (bottom) and ^{208}Pb (top) ions is observed.

been reported in Ref. [36], based on the combination of four experiments carried out at four different laboratories. Proton- and neutron-transfer reactions, neutron capture on a highly radioactive ^{63}Ni (2 GBq) target, nuclear resonance fluorescence, and Coulomb excitation had to be measured to reach the sensitivity required to probe shape coexistence in ^{64}Ni . As such, some of the results reported here were first introduced in Ref. [36] as part of the experimental evidence supporting the interpretation in terms of triple shape coexistence.

II. EXPERIMENT AND ANALYSIS

Multistep Coulomb excitation of the nucleus ^{64}Ni was performed at the ATLAS facility at Argonne National Laboratory, where a 0.5 mg/cm^2 isotopically enriched ^{208}Pb target, with a $6\text{-}\mu\text{g/cm}^2$ Al front layer and a $40\text{-}\mu\text{g/cm}^2$ C backing, was bombarded by a ^{64}Ni beam at an energy of 272 MeV, a value 14% below the Coulomb barrier. Gamma rays of interest were detected with the GRETTINA tracking array [37] in coincidence with the two reaction partners measured by the CHICO2 compact heavy ion counter [38]. At the time of this experiment, 12 GRETTINA modules were available, providing a total of 48 highly segmented coaxial HPGc crystals. The 20 position-sensitive parallel-plate avalanche counters of CHICO2, arranged symmetrically around the beam axis, covered 68% of the solid angle around the target with resolutions (FWHM) of 1.6° and 2.5° or better in the polar (θ) and azimuthal (ϕ) angles, relative to the beam axis. Figure 1 illustrates the ability of CHICO2 to discriminate between the two reaction partners in a plot of the difference in their time of flight, ΔT_{tof} , as a function of the scattering angle. A time resolution (FWHM) of ~ 1.2 ns was achieved in this measurement, and the mass resolution, $\Delta M/M$, was determined to be about 5%.

With CHICO2, the trajectories of the reaction partners could be determined on an event-by-event basis. These were subsequently used in the precise correction of the γ rays for the Doppler shift. Figure 2 presents the spectrum measured in coincidence with ^{64}Ni projectiles: the γ rays can be associated

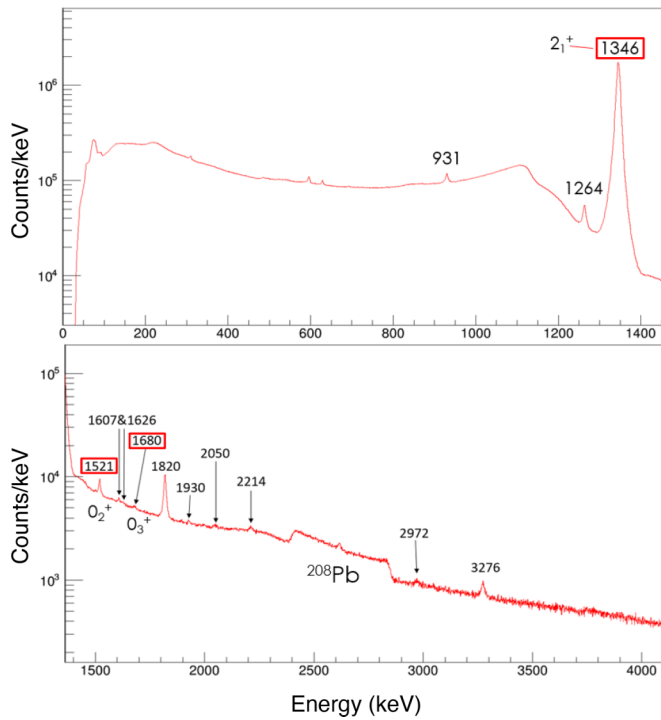


FIG. 2. Total γ -ray spectrum obtained from Coulomb excitation, encompassing the full azimuthal range for CHICO2. The spectrum has been corrected for the Doppler shift assuming ^{64}Ni kinematics. All labeled γ rays are associated with transitions in ^{64}Ni . The three most significant transitions for the present discussion are placed in boxes and correspond to the $2_1^+ \rightarrow 0_1^+$, $0_2^+ \rightarrow 2_1^+$, and $0_3^+ \rightarrow 2_1^+$ transitions, respectively.

with known transitions in ^{64}Ni [34,39] with the exception of the broad bump at around 2.6 MeV. The latter corresponds to the ^{208}Pb $3_1^- \rightarrow 0_1^+$ ground-state transition for which the Doppler shift correction is inappropriate. The level scheme of

TABLE I. Literature branching and mixing ratios as well as lifetimes for selected transitions used in constraining the χ^2 minimization in GOSIA. The lifetime data was taken from Ref. [41]. All others are from ENSDF [39].

Branching ratio	Value	
	Literature	GOSIA
$(2_3^+) \rightarrow 0_1^+ / (2_3^+) \rightarrow 2_1^+$	0.6(2)	0.61
$(2_3^+) \rightarrow 2_2^+ / (2_3^+) \rightarrow 2_1^+$	0.8(3)	0.63
$2_6^+ \rightarrow 2_1^+ / 2_6^+ \rightarrow 0_1^+$	0.33(10)	0.38
Mixing ratio		
$2_2^+ \rightarrow 2_1^+$	0.75(20)	0.69
Lifetime (ps)		
2_1^+	1.29(5)	1.28

Fig. 3 identifies all the ^{64}Ni transitions observed in the present work.

For the analysis, γ -ray spectra were obtained for seven ranges of the ^{64}Ni scattering angle: $30^\circ - 40^\circ$, $40^\circ - 50^\circ$, $50^\circ - 60^\circ$, $60^\circ - 70^\circ$, $70^\circ - 80^\circ$, $96^\circ - 130^\circ$, and $130^\circ - 160^\circ$, in order to study the dependence of the Coulomb excitation probabilities on scattering angle. As is customary for this type of measurement, the intensities of all the transitions in Fig. 2 were extracted for each angular range and corrected for both the detector efficiency and the geometry of the experimental setup. The resulting yields were subsequently analyzed with the semiclassical Coulomb excitation code, GOSIA [40], a coupled-channel, least-squares fit code which derives matrix elements from a standard χ^2 analysis. The electromagnetic matrix elements of interest are parameters in a procedure comparing the measured γ -ray yields with calculated ones. At the onset, known $B(E2)$ probabilities, lifetimes, branching, and mixing ratios [34,39], summarized in Table I, were included as constraints of the relevant pa-

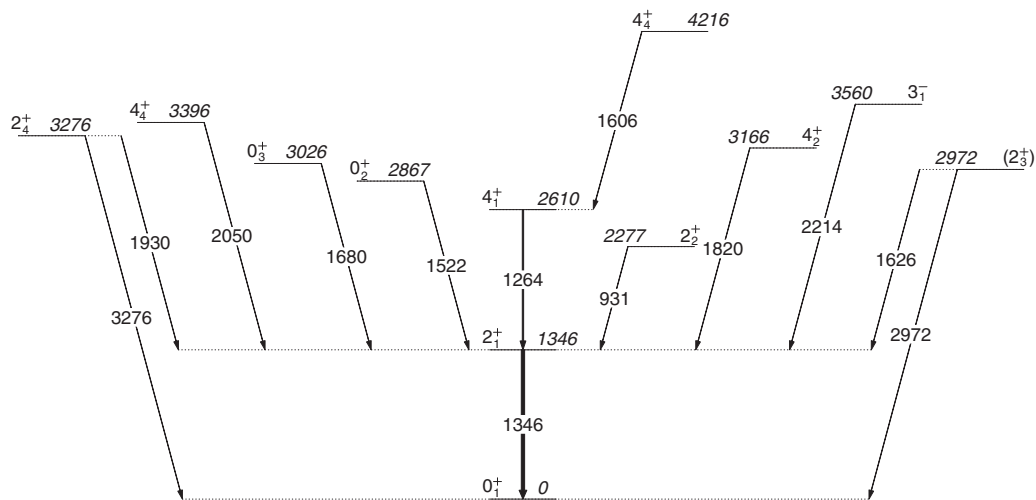


FIG. 3. Level scheme depicting all 13 known ^{64}Ni transitions observed in this Coulomb excitation experiment. Parentheses indicate tentative spin-parity assignments. The subscripts on the spin quantum numbers refer to the sequence in which levels of the same spin and parity are observed in this work.

TABLE II. Summary of $E1$, $E2$, and $M1$ matrix elements and reduced transition probabilities for ^{64}Ni deduced in the present work. Units for reduced transition strengths are μ_N^2 , $e^2 \text{fm}^2$, and $e^2 \text{fm}^4$ for $M1$, $E1$, and $E2$ transitions, respectively. Accordingly, $E1$, $E2$, and $M1$ matrix elements are listed in units of $eb^{1/2}$, eb , and μ_N . Here, λ is either E or M and L takes values of 1 or 2. The last column presents the reduced transition probabilities in Weisskopf units (W.u.). Note that the uncertainties are quoted in a format based on whether the errors are symmetric or not.

E (keV)	$I_i^\pi \rightarrow I_f^\pi$	Mult (λL)	E_γ (keV)	$\langle i M(\lambda L) f\rangle$	$B(\lambda L \downarrow; i \rightarrow f)$	$B(\lambda L \downarrow; i \rightarrow f)$ (W.u.)
1346	$2_1^+ \rightarrow 0_1^+$	$E2$	1346	0.268(16)	144(18)	9.5(12)
2277	$2_2^+ \rightarrow 0_1^+$	$E2$		$0.005_{-0.001}^{+0.002}$	$0.05_{-0.02}^{+0.05}$	$0.003_{-0.001}^{+0.003}$
2277	$2_2^+ \rightarrow 2_1^+$	$E2$	931	$0.149_{-0.004}^{+0.007}$	44_{-2}^{+4a}	$2.9_{-0.2}^{+0.3}$
2277	$2_2^+ \rightarrow 2_1^+$	$M1$	931	1_{-3}^{+1}	$0.2_{-0.2}^{+0.6}$	$0.11_{-0.11}^{+0.34}$
2610	$4_1^+ \rightarrow 2_1^+$	$E2$	1264	$0.244_{-0.008}^{+0.013}$	66_{-4}^{+7}	4.4_{-3}^{+5}
2610	$4_1^+ \rightarrow 2_2^+$	$E2$		$0.42_{-0.03}^{+0.05}$	196_{-28}^{+47}	13_{-2}^{+3}
2867	$0_2^+ \rightarrow 2_1^+$	$E2$	1522	0.070(2)	49(3)	3.2(2)
2867	$0_2^+ \rightarrow 2_2^+$	$E2$		0.27(4)	729(216)	48(14)
2972	$(2_3^+) \rightarrow 0_1^+$	$E2$	2972	0.009(1)	0.16(4)	0.011(2)
2972	$(2_3^+) \rightarrow 2_1^+$	$E2$	1626	0.05(2)	5_{-3}^{+5}	$0.3_{-0.2}^{+0.3}$
2972	$(2_3^+) \rightarrow 2_1^+$	$M1$	1626	$-0.003_{-0.033}^{+0.041}$	$0.000002_{-0.000002}^{+0.0003854}$	$0.000001_{-0.000001}^{+0.000215}$
2972	$(2_3^+) \rightarrow 2_2^+$	$E2$		$0.03_{-0.07}^{+0.08}$	$1.8_{-1.8}^{+22.4}$	$0.12_{-0.12}^{+1.58}$
2972	$(2_3^+) \rightarrow 2_2^+$	$M1$		$-0.19_{-0.08}^{+0.04}$	$0.007_{-0.006}^{+0.003}$	$0.004_{-0.003}^{+0.002}$
2972	$(2_3^+) \rightarrow 4_1^+$	$E2$		0.26(5)	135(52)	9(4)
3026	$0_3^+ \rightarrow 2_1^+$	$E2$	1680	0.030(2)	9.0(12)	0.59(8)
3026	$0_3^+ \rightarrow 2_2^+$	$E2$		$0.25_{-0.07}^{+0.05}$	625_{-350}^{+250}	41_{-23}^{+16}
3166	$4_2^+ \rightarrow 2_1^+$	$E2$	1820	0.249(4)	68.9(22)	4.5(2)
3276	$2_4^+ \rightarrow 0_1^+$	$E2$	3276	0.030(2)	1.80(24)	0.12(2)
3276	$2_4^+ \rightarrow 2_1^+$	$E2$	1930	-0.069(5)	9.5(1.7)	0.63(9)
3276	$2_4^+ \rightarrow 2_1^+$	$M1$	1930	$0.02_{-0.05}^{+0.03}$	$0.00008_{-0.00008}^{+0.00042}$	$0.00005_{-0.00005}^{+0.00024}$
3396	$4_3^+ \rightarrow 2_1^+$	$E2$	2050	0.047(5)	2.5(5)	0.16(3)
3560	$3_1^- \rightarrow 2_1^+$	$E1$	2214	0.035(6)	0.018(6)	0.017(6)
4216	$4_4^+ \rightarrow 2_1^+$	$E2$		0.101(7)	11.3(16)	0.8(1)
4216	$4_4^+ \rightarrow 4_1^+$	$E2$	1606	$-0.9_{-0.1}^{+0.7}$	900_{-200}^{+1944}	59_{-13}^{+128}
4216	$4_4^+ \rightarrow 4_1^+$	$M1$	1606	$1.3_{-3.0}^{+0.5}$	$0.19_{-0.19}^{+0.17}$	$0.11_{-0.11}^{+0.10}$

^aThe value of 73(8) eb previously quoted for this transition in Ref. [36] is in error. The present value of 44_{-2}^{+4} eb is correct.

rameters. Note that the Coulomb excitation analysis only considers relative yields, e.g., all yields are normalized to that of the 1346-keV $2_1^+ \rightarrow 0_1^+$ transition. The final transition and diagonal matrix elements, together with associated errors, can be found in Tables II and III, respectively.

TABLE III. Summary of diagonal matrix elements along with the associated spectroscopic (Q) quadrupole moments in units of eb for ^{64}Ni low-lying states deduced in the present work.

E_{level} (keV)	I^π	$\langle I_i M(E2) I_f\rangle$	Q_s
1346	2_1^+	0.11(3)	+0.08(2)
2276	2_2^+	$0.30_{-0.05}^{+0.03}$	$+0.23_{-0.04}^{+0.02}$
2610	4_1^+	$-0.4_{-0.3}^{+0.1}$	$-0.30_{-0.23}^{+0.08}$
3166	4_2^+	$0.1_{-0.3}^{+0.1}$	$+0.08_{-0.23}^{+0.08}$

III. RESULTS

The level scheme displayed in Fig. 3 contains the 13 transitions observed in the experiment. Ten of these were reported in Ref. [34], the most recent work on ^{64}Ni , where excited states were populated in quasielastic and deep-inelastic reactions of a 430-MeV ^{64}Ni beam on a thick ^{238}U target. The three additional γ rays placed in Fig. 3 are the 1606-keV transition originating from a 4216-keV, 4^+ state and two transitions of 1930 and 3276 keV linking an excited 2^+ , 3276-keV level with the 2_1^+ and ground states, respectively. These three transitions had also been observed previously [39]. In the context of this paper, the observation of the 1522- and 1680-keV γ rays linking the 2867- and 3026-keV 0^+ excitations to the 2_1^+ yrast state are particularly noteworthy, as these two levels could possibly be associated with different ^{64}Ni minima within the type-II shell evolution picture described above. Furthermore, when comparing the present data with those from the in-beam work of Ref. [34], it is worth noting

TABLE IV. Comparison of level lifetimes determined in the present work with the adopted values taken from the ENSDF database [39].

E (keV)	I^π	Lifetime (ps)	
		ENSDF	Present work
1346	2_1^+	1.57(5)	1.28(16)
2610	4_1^+	2.5(4)	2.13(23)
2867	0_2^+	2.09(14)	2.04(13)
2972	2_3^+	$0.19^{+0.19}_{-0.07}$	2.58(12)
3026	0_3^+	5.2(17)	6.5(9)
3276	2_4^+	0.35(4)	1.1(8)

the difference in the general feeding pattern of observed levels in both measurements with Coulomb excitation populating low-spin, non-yrast states considerably more strongly than is the case following complex reactions above the barrier.

The transition matrix elements, reduced transition probabilities, and their associated uncertainties are displayed in Table II, while Table III presents the static matrix elements for the four lowest-lying states along with the corresponding spectroscopic quadrupole moments. At the onset of the minimization process, the matrix element for the excitation of the 2_1^+ level from the ground state was kept fixed at the value reported by Allmond *et al.* [41] following single-step Coulomb excitation of the $^{64}\text{Ni} + ^{12}\text{C}$ system. Once the χ^2 minimum for the full data set was determined, this constraint was removed for subsequent minimizations. The latter were used to determine the correlated uncertainties. The value of 0.268(16) *eb* reported in Table II for the $\langle 0_1^+ | M(E2) | 2_1^+ \rangle$ matrix element agrees with the 0.268(5) *eb* one of Ref. [41], herewith providing confidence in the results of the present analysis. This confidence is further validated by the agreement between the literature data included as constraints in the minimization and the experimentally deduced values (Table I). No Coulomb excitation data for other higher-lying ^{64}Ni states was available prior to this work. However, a $B(E2; 4_1^+ \rightarrow 2_1^+)$ transition probability of 6.6 (1.0) Weisskopf units (W.u.) was extracted from a lifetime measurement carried out in conjunction with a *g*-factor determination [42]. This value is of the same order as the 4.4^{+5}_{-3} W.u. value obtained in the present study. Comparisons are extended further in Table IV, where adopted level lifetimes from the evaluated nuclear structure data file (ENSDF) database [39] are compared with corresponding values derived from the present measurement. It can be seen that the agreement between the two data sets is satisfactory, with values of the same order of magnitude in each case as well as similar trends as a function of level energy. Overall, all the measured $B(E2)$ transition probabilities displayed in Table II correspond to values of the order of a few single-particle units ($\sim 1 - 10$ W.u.), consistent with noncollective excitations.

IV. DISCUSSION

The present ^{64}Ni data have been compared with three different sets of shell-model calculations. The first of these,

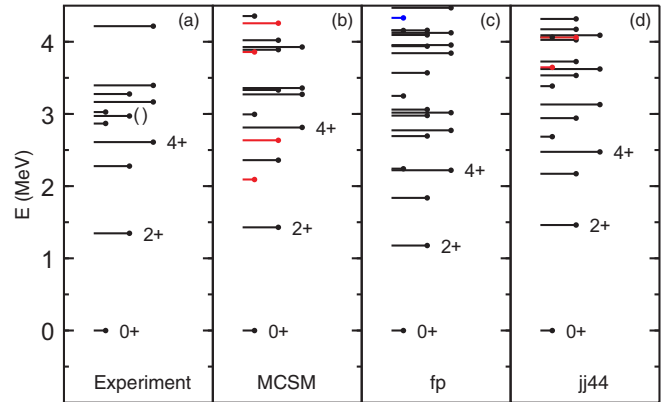


FIG. 4. Comparison of the results of jj44, fp, and MCSM excitation energy calculations with the ^{64}Ni states observed in the present Coulomb excitation experiment. Calculated positive-parity levels with spin 0, 2, and 4 up to 4.5 MeV are included. The length of the horizontal lines indicates the spin value. The red lines in the MCSM panel indicate states with relatively large occupancies of $g_{9/2}$ neutron particles and $f_{7/2}$ proton holes. The blue line in the fp panel indicates the first level with a relatively large number of $f_{7/2}$ proton holes, while the red lines in the jj44 panel signal states with a large $g_{9/2}$ neutron occupancy.

labeled as jj44, is aimed specifically at exploring the role of neutron multi particle-hole excitations from the fp shell into the $g_{9/2}$ orbital. Thus, the model space is comprised of the $f_{5/2}$, $p_{3/2}$, $p_{1/2}$, and $g_{9/2}$ neutron states, and the Hamiltonian incorporates the jj44pna effective interaction proposed by Lisetskiy *et al.* [43]. The latter is based on an analysis and fit of experimental data on the $^{57-78}\text{Ni}$ isotopes as well as on those for the $^{77}\text{Cu} - ^{100}\text{Sn}$ isotones available at the time (2004). In addition, the role of excitations involving both protons and neutrons was investigated in calculations within the $f_{7/2}$, $f_{5/2}$, $p_{3/2}$, and $p_{1/2}$ model space with a Hamiltonian including the GXPF1A effective interaction [44]. This interaction has been fine-tuned on large data sets in fp -shell nuclei, and has proved successful in reproducing many structural properties in $A = 40 - 70$ isotopes ranging from Ca to Ni, including the onset of new neutron subshell closures at $N = 32$ and 34 [44–46]. Calculations with this interaction are labeled as fp hereafter. Finally, a more global view of excitations in ^{64}Ni was attempted with calculations within the Monte Carlo shell-model framework (MCSM) of Refs. [12,47–49]. These calculations are of the same type as those presented earlier for $^{66-78}\text{Ni}$ [8,12]. In this case, however, the model space encompasses protons and neutrons in the full fp shell with, in addition, the $g_{9/2}$ and $d_{5/2}$ orbitals. The Hamiltonian is based on the modified A3DA effective interaction used for comparisons with data, for example, on neutron-rich Ni isotopes in Refs. [5,6,8].

A comparison between the level energies observed in the present work and the results of the various calculations is presented in Figs. 4(a)–4(d). Note that negative-parity states dominate the structure of ^{64}Ni above the 4^+ levels [34]. These excitations were not observed in the present work, with the exception of the 3560-keV 3_1^- state which is included in Fig. 3. Hence they will not be discussed here beyond

stating that they are understood as involving mostly one-neutron particle-hole excitations from the fp shell to the $g_{9/2}$ orbital, based on the shell-model calculations presented in Ref. [34], and those carried out for the present work within the $jj44pna$ Hamiltonian (not shown).

The two more conventional shell-model calculations of the positive-parity states ($jj44$ and fp) reproduced the data rather well: see Figs. 4(c) and 4(d). Quantitatively, results of the former with the $jj44pna$ interaction appear to reproduce the data somewhat better, with a rms deviation of 242 keV for the states observed in the present study. The corresponding value for the fp results, obtained with the $GXPFI1A$ interaction, is 314 keV. Furthermore, the sequence of levels as a function of spin and excitation energy is reproduced more closely in the $jj44$ computations. Thus, starting from the 0^+ ground state, two 2^+ levels are computed to lie lower than the first 4^+ excitation, which is in turn followed by the 0_2^+ state. It is worth pointing out that the agreement between data and calculations for the 0_3^+ level is worse than that for the 0_2^+ state, as the former is computed nearly 359 keV too high in excitation energy while the latter is predicted to lie lower by only 182 keV. The $jj44$ results also predict the 0_3^+ state to be higher in excitation energy than the 4_2^+ level, a result at variance with the data. Within the fp approach, the 0_2^+ level is calculated 630 keV too low, but agreement between data and theory is more satisfactory for the 0_3^+ state, with calculations locating the excitation 215 keV higher. However, the fp Hamiltonian places a number of 2^+ and 4^+ states below the 0_3^+ level, a feature not exhibited by the data. More generally, from Fig. 4(c) it is clear that the fp level sequence is compressed with respect to the data. This is likely due to the increasing role of neutron pairing brought about by the presence of the $g_{9/2}$ orbital close to the Fermi surface as one approaches ^{68}Ni .

Figure 4(b) provides similar comparisons between the measured and calculated level structures, but within the MCSM framework. In this instance, the 298-keV rms deviation is comparable to those reported above and well within the level of accuracy to be expected for any of the three calculations. Here as well, the computed states give rise to a spin sequence with less similarity to the data. For example, the 0_2^+ state is predicted almost 780 keV too low, while the calculated 0_3^+ excitation is low as well, although only by 30 keV. Furthermore, the 0_2^+ level is calculated to lie lower than the 2_2^+ state, and the ordering of the 2_3^+ and 4_1^+ levels is reversed as well.

Since ^{64}Ni possesses a closed major proton shell, it was thought *a priori* [34] that most of the low-energy states would be associated predominantly with neutron excitations. This is supported by the relative success of the $jj44$ calculations. However, a closer look at the 0_3^+ state, specifically, indicates that this level is, in fact, reproduced best by the MCSM calculations, followed by the fp ones, and that the deviation is largest in the $jj44$ space. This suggests that the configuration of the 0_3^+ level involves a combination of both proton and neutron excitations rather than the expected dominant neutron ones, which reproduce the other low-spin states. The configurations dominated by two neutrons in the $g_{9/2}$ orbital [red lines in panels (b) and (d) of Fig. 4] start at 2.1 MeV for the MCSM calculations and 3.7 MeV in the case of $jj44$ computations.

Comparison with the experimental energies suggests that the $(\nu g_{9/2})^2$ configurations start near 3 MeV.

Tables V and VI list the measured strengths and spectroscopic quadrupole moments alongside those obtained from the two shell-model calculations within the $jj44$ and fp model spaces as well as from the MCSM approach. Transitions for which an experimental value is not listed in the table were not determined via the analysis with GOSIA, but the calculated values are included due to their relevance for the ensuing discussion. As noted above, decays involving the 3_1^- level at 3560 keV are not listed, as the three calculations have not been extended to the negative-parity states. However, the decay from this state to the 2_1^+ level is characterized by an $E1$ transition strength of only 0.0170(2) W.u., strongly implying single-particle character. This strength is also comparable to those of similar $3^- \rightarrow 2_1^+$ transitions in the other even Ni isotopes: they are all of the order of a few mW.u. [50]. It is noted that while all three calculations correctly predict a positive quadrupole moment for the 2_1^+ state, only the fp computation, and to a lesser extent, the $jj44$ interaction are able to provide a better agreement with the experimental data in terms of the absolute magnitude. All three values are, however, consistent with a near-spherical ground state. In contrast, the large magnitude and positive sign determined experimentally for the $Q_s(2_2^+)$ moment are not reproduced in any of the three calculations.

A. Transition probabilities and occupancies for the 2^+ states

The computations of reduced transition probabilities within the shell model require the use of effective charges. All three calculations adopt the conventional value of $e_p = 1.5e$ for the proton effective charge. However, while the MCSM and fp computations also adopt the canonical $0.5e$ value for the neutron effective charge, the $jj44$ ones use $e_n = 1.2e$. As stated above, the $jj44$ calculations only consider neutron excitations, including those involving neutrons in the $g_{9/2}$ orbital. As protons are ignored in this case, their contribution to the $B(E2)$ value is mimicked by boosting e_n to the value required to reproduce the $B(E2; 2_1^+ \rightarrow 0_1^+)$ transition probability.

The strength of the 1346-keV ground-state transition is computed satisfactorily as the measured value of $144(18) e^2 \text{fm}^4$ is reproduced within errors by all three calculations (see Table V). This result is significant only for the fp and MCSM calculations, as they are carried out with the standard effective charges. In fact, this agreement can be viewed as reinforcing confidence in the present data. In the case of the $jj44$ computations, the calculated $142.5 e^2 \text{fm}^4$ value solely reflects the fact that the adjustment of the neutron effective charge seems appropriate. An inspection of the occupancies in the three calculations (see Table VII) reveals that the proton $f_{7/2,5/2}$, $p_{3/2,1/2}$ configurations in the fp and MCSM spaces are similar for the 2_1^+ level; e.g., the $\pi g_{9/2}$ and the $\nu g_{9/2}$ and $\nu d_{5/2}$ occupations are found to be negligible in the MCSM approach. It is worth noting that this observation of a small occupation of proton orbitals across the shell gap is valid for all the levels discussed in the present work. Furthermore, the respective neutron occupancies in the MCSM and fp results are similar in the 0_1^+ and in the 2_1^+ levels. Hence, no significant

TABLE V. Comparison of experimental reduced transition strengths with those obtained via fp, jj44, and MCSM calculations. Units for reduced transition strengths are μ_N^2 and $e^2 \text{fm}^4$ for M1 and E2 transitions, respectively. Here, λ is either E or M and L takes values of 1 or 2.

$I_i^\pi \rightarrow I_f^\pi$	Mult (λL)	E_γ (keV)	$B(\lambda L \downarrow; i \rightarrow f)$			
			Exp	fp	jj44	MCSM
$2_1^+ \rightarrow 0_1^+$	E2	1346	144(18)	139.0	142.5	158.9
$2_2^+ \rightarrow 0_1^+$	E2		$0.05_{-0.02}^{+0.05}$	2.0	2.2	0.49
$2_2^+ \rightarrow 2_1^+$	E2	931	44_{-2}^{+4}	139.6	185.9	127.3
$2_2^+ \rightarrow 2_1^+$	M1	931	$0.2_{-0.2}^{+0.6}$	0.014	0.011	0.011
$4_1^+ \rightarrow 2_1^+$	E2	1264	66_{-4}^{+7}	28.9	0.22	138.5
$4_1^+ \rightarrow 2_2^+$	E2		196_{-28}^{+47}	61.5	43.2	88.5
$0_2^+ \rightarrow 2_1^+$	E2	1522	49(3)	70.9	1.8	182.4
$0_2^+ \rightarrow 2_2^+$	E2		729(216)	69.2	21.9	695.7
$(2_3^+) \rightarrow 0_1^+$	E2	2972	0.16(4)	7.4	0.25	0.28
$(2_3^+) \rightarrow 2_1^+$	E2	1626	5_{-3}^{+5}	20.2	6.2	0.10
$(2_3^+) \rightarrow 2_1^+$	M1	1626	$0.000002_{-0.000002}^{+0.000385}$	0.026	0.0054	0.00001
$(2_3^+) \rightarrow 2_2^+$	E2		$1.8_{-1.8}^{+22.4}$	7.7	1.4	161.8
$(2_3^+) \rightarrow 2_2^+$	M1		$0.007_{-0.006}^{+0.003}$	0.028	0.067	0.001
$(2_3^+) \rightarrow 4_1^+$	E2		135(52)	0.48	11.5	20.2
$0_3^+ \rightarrow 2_1^+$	E2	1680	9.0(12)	0.21	1.5	36.2
$0_3^+ \rightarrow 2_2^+$	E2		625_{-350}^{+250}	31.9	2.1	6.1
$4_2^+ \rightarrow 2_1^+$	E2	1820	68.9(22)	133.7	140.1	114.7
$4_2^+ \rightarrow 2_2^+$	E2			2.8	2.1	14.7
$2_4^+ \rightarrow 0_1^+$	E2	3276	1.80(24)	2.4	0.006	5.7
$2_4^+ \rightarrow 2_1^+$	E2	1930	9.5(1.7)	11.2	0.2	11.3
$2_4^+ \rightarrow 2_1^+$	M1	1930	$0.00008_{-0.00008}^{+0.00042}$	0.0022	0.000009	0.011
$4_3^+ \rightarrow 2_1^+$	E2	2050	2.5(5)	8.2	10.1	6.2
$4_3^+ \rightarrow 2_2^+$	E2			3.9	0.06	120.1
$4_3^+ \rightarrow 4_2^+$	E2			24.6	9.6	108.1
$4_4^+ \rightarrow 2_1^+$	E2		11.3(16)	3.8	1.9	1.8
$4_4^+ \rightarrow 4_1^+$	E2	1606	900_{-200}^{+1944}	1.7	5.4	0.08
$4_4^+ \rightarrow 4_1^+$	M1	1606	$0.19_{-0.19}^{+0.17}$	0.34	0.018	0.0079

difference between these two calculated strengths should be expected. In addition, the neutron occupancies in the MCSM and jj44 calculations are similar as well, with the $\nu g_{9/2}$ orbital occupancy in the wave function at only ~ 0.6 .

The $2_2^+ \rightarrow 0_1^+$ transition strength is experimentally determined to be quite small, with a value of $0.05_{-0.02}^{+0.04} e^2 \text{fm}^4$.

TABLE VI. Experimental spectroscopic quadrupole moments, Q_s , for low-lying states in ^{64}Ni in comparison with results of the shell-model calculations discussed in the text.

E_{level} (keV)	I^π	Q_s (eb)	fp	jj44	MCSM
1346	2_1^+	+0.08(2)	+0.12	+0.04	+0.20
2276	2_2^+	$+0.23_{-0.04}^{+0.02}$	-0.10	-0.02	-0.03
2610	4_1^+	$-0.30_{-0.23}^{+0.08}$	+0.29	+0.26	+0.35
3166	4_2^+	$+0.08_{-0.23}^{+0.08}$	+0.08	+0.14	+0.27

Indeed, all three calculations reproduce this value rather well, with the MCSM one matching it best with a strength of $0.49 e^2 \text{fm}^4$. For the $2_2^+ \rightarrow 2_1^+$ transition, the strengths determined by all three calculations are larger than that to the ground state. They are also larger than the $44_{-2}^{+4} e^2 \text{fm}^4$ measured value. While the fp and MCSM strengths are comparable in this case, the jj44 calculation overpredicts the value even more, computing a strength of $185.9 e^2 \text{fm}^4$. This overprediction is likely due to the artificially large effective charge of the neutrons applied in the jj44 calculations. Hence, this overprediction in comparison to the other two values also suggests that the majority of the wave functions involved in the 2_1^+ and 2_2^+ levels occur within the fp space. Moreover, all three calculations also reproduce small M1 values similar to the small $0.1_{-0.1}^{+0.6} \mu_n^2$ value observed experimentally.

A closer examination of the neutron occupancies for the 2_2^+ level reveal a general agreement between all three

TABLE VII. Orbital occupancy values associated with 2^+ states in ^{64}Ni , as predicted by the fp, jj44, and MCSM calculations. The occupancy values for the 0_1^+ state are included for reference. All proton occupancy values correspond to zero for the jj44 computation due to the fact that proton excitations were excluded from the model space (see text for details).

I^π	Calculation	π					ν				
		$f_{7/2}$	$p_{3/2}$	$f_{5/2}$	$p_{1/2}$	$g_{9/2}$	$f_{7/2}$	$p_{3/2}$	$f_{5/2}$	$p_{1/2}$	$g_{9/2}$
0_1^+	fp	7.51	0.37	0.1	0.03		7.92	3.22	4.03	0.83	
	jj44							3.04	3.57	0.74	0.65
	MCSM	7.35	0.40	0.1	0.03	0.10	7.84	3.14	3.58	0.82	0.58
2_1^+	fp	7.38	0.48	0.1	0.03		7.92	3.22	4.03	0.83	
	jj44							3.04	3.57	0.74	0.65
	MCSM	7.1	0.59	0.14	0.05	0.10	7.82	3.10	3.31	1.07	0.66
2_2^+	fp	7.41	0.46	0.1	0.03		7.94	3.4	3.83	0.84	
	jj44							3.12	3.57	0.92	0.39
	MCSM	7.0	0.65	0.19	0.07	0.09	7.80	3.05	3.47	0.87	0.77
2_3^+	fp	7.41	0.44	1	0.03		7.94	3.36	3.62	1.08	
	jj44							2.24	4.88	0.26	0.62
	MCSM	6.38	1.04	0.34	0.14	0.09	7.69	2.68	3.05	1.16	1.39
2_4^+	fp	7.58	0.32	0.09	0.02		7.93	2.12	4.19	0.77	
	jj44							3.24	3.24	1.11	0.41
	MCSM	7.33	0.44	0.09	0.03	0.09	7.86	3.19	3.47	1.09	0.36

computations. The most significant differences between the MCSM calculations and the conventional shell-model approaches appear to be slight reductions in the $f_{7/2,5/2}$ and $p_{3/2}$ MCSM occupancies, compensated by a larger occupancy of the $g_{9/2}$ neutron orbital. The MCSM value of 0.77 for this $g_{9/2}$ occupation number is larger than the analogous value of 0.39 in the jj44 space, indicating that this increase in occupancy is likely one of the main disparities between the wave functions associated with the 2_2^+ level and the 0_1^+ state. Additionally, while the occupation numbers for the proton orbitals remain mostly unchanged between the 2_2^+ level and the ground state in the fp space, and the MCSM values agree for the most part with those of the fp calculations, the MCSM occupancies still indicate some movement of protons from the $f_{7/2}$ to the $p_{3/2}$ orbital. Hence, the calculations of the $2_2^+ \rightarrow 0_1^+$ transition strength indicate that proton excitations may play a minor role in the 2_2^+ wave function.

A rather small transition strength of $0.16(4) e^2 \text{fm}^4$ was measured for the $2_3^+ \rightarrow 0_1^+$ transition, which both the MCSM and jj44 calculations reflect well (see Table V). The fp calculation, on the other hand, produces a considerably larger value of $7.4 e^2 \text{fm}^4$, suggesting that this transition is likely dominated by neutron excitations outside the fp model space. This interpretation is supported by the measured strength of the $2_3^+ \rightarrow 2_1^+$ transition, which is calculated well by both the MCSM and jj44 computations but, once again, over-predicted by the fp calculations. The small $M1$ transition strength further emphasizes the prevalence of neutron excitations. The small experimental $2_3^+ \rightarrow 2_2^+$ transition strength of $1.8_{-8.4}^{+9.6} e^2 \text{fm}^4$ is predicted reasonably well by the fp calculations and even more so by the jj44 ones, whereas the MCSM result drastically overshoots, predicting a value of $161.8 e^2 \text{fm}^4$. Here, not much more is revealed by the weak $B(M1)$ transition. The final decay mode involving the 2_3^+ level worth noting is the $2_3^+ \rightarrow 4_1^+$ transition. The large experimen-

tally determined strength of $135(52) e^2 \text{fm}^4$ is best reproduced by the jj44 and MCSM calculations but with significantly smaller values of 11.5 and $20.2 e^2 \text{fm}^4$, respectively, whereas the fp value of $0.42 e^2 \text{fm}^4$ is even lower. From the deexcitation pattern of the 2_3^+ level, it appears that this state is dominated by neutron excitations and probably involves the $g_{9/2}$ intruder orbital.

The proton occupancies for the 2_3^+ state differ somewhat between the fp and MCSM calculations, with the MCSM results indicating a drop in the $f_{7/2}$ occupation number and a redistribution of protons, predominantly to the $p_{3/2}$ orbital. Similar to the 2_2^+ level, the MCSM results predict a relatively high contribution from the neutron $g_{9/2}$ orbital (1.39 neutrons). Notably, the jj44 occupancies display a significant drop in both p orbitals and an increase in the $f_{5/2}$ one, in addition to the $g_{9/2}$ occupancy. This suggests that it is likely the larger neutron occupancy that brings the MCSM calculations in agreement with the observed $2_3^+ \rightarrow 0_1^+$ transition strength. The $2_3^+ \rightarrow 2_2^+$ decay branch, on the other hand, is more challenging to comprehend by following the same reasoning. It is understandable in the jj44 calculations that the disparity in the occupancy of the $g_{9/2}$ orbital between the two states would lead to a smaller transition strength. However, assuming that this applies for neutrons in the MCSM result as well, it must then be concluded that the rearrangement of the protons in the MCSM case (with respect to the fp one) leads to such a large effect in the transition strength.

The measured strength of $1.80(24) e^2 \text{fm}^4$ for the $2_4^+ \rightarrow 0_1^+$ transition is well reproduced by both fp and MCSM calculations, while the jj44 value, corresponding to $0.006 e^2 \text{fm}^4$, appears to be too small and thus argues for the strength being associated with excitations predominantly within the fp space. The same conclusion is reached for the $2_4^+ \rightarrow 2_1^+$ transition, with the fp and MCSM calculations, once again, closely predicting the observed value of $9.5(1.7) e^2 \text{fm}^4$, while

the jj44 computation provides too small a value ($0.2 e^2 \text{fm}^4$). Unfortunately, the $M1$ transition strength does not reveal much in this case, as each set of calculations predicts it to be quite small. The proton occupancies of the 2_4^+ level with respect to that of the ground state are nearly the same for both the fp and MCSM calculations, suggesting that the difference in wave functions between the two levels largely arises from neutron contributions. In terms of neutron occupancies, the fp calculations compute a drop in the $p_{3/2}$ neutron number, while the MCSM calculations do not. Instead they indicate a drop in the $g_{9/2}$ orbital occupancy with respect to the ground state. However, the fact that the fp value reproduces the data well in this case may indicate that $g_{9/2}$ orbital excitations do not play as significant a role in this state, and that, instead, the redistribution of neutrons to the $p_{3/2}$ orbital may be more relevant. With respect to the 2_1^+ level, both fp and MCSM calculations predict a small reorganization of protons from the $p_{3/2}$ state back to the $f_{7/2}$ orbital, but, for the most part, the proton occupancies remain quite similar between the two states. From the considerations above, it can be concluded that the 2_4^+ level corresponds to an excitation within the fp shell.

A trend similar to that discussed for the 2^+ states is observed for the four 4^+ levels populated in the present study, but these are not all discussed here. Rather, a detailed analysis of their configurations and occupancies can be found in Ref. [51]. The calculations all indicate that the low-lying levels in ^{64}Ni are dominated by excitations involving the $\nu(f_{5/2}, p_{3/2}, p_{1/2})^8$ neutron configuration so that, to first order, the $B(E2)$ transition probabilities computed within the fp and jj44 model spaces would be expected to be similar, except for an overall scaling factor coming from the excitation of a $f_{7/2}$ proton into the $\pi(f_{5/2}, p_{3/2}, p_{1/2})$ configuration. This expectation is not borne out for the $B(E2; 4_1^+ \rightarrow 2_1^+)$ probability (Table V) where the fp calculations are in better agreement with experiment, herewith indicating that the effective Hamiltonians within the $\nu(f_{5/2}, p_{3/2}, p_{1/2})^8$ model space are still different for the two interactions. In the case of the $4_1^+ \rightarrow 2_1^+$ $E2$ matrix element, the difference can be attributed to a large canceling contribution involving $f_{5/2}$ neutrons [51], which is absent in the fp model.

B. Transition probabilities and occupancies for the 0^+ states

The main focus of this work is on the nature of the excited 0^+ states and their relationships with the 2^+ and 4^+ levels. In this regard, both the MCSM and fp interactions provide strong indications about the nature of the 0_2^+ state. The measured strength of $49(3) e^2 \text{fm}^4$ for the $0_2^+ \rightarrow 2_1^+$ transition is relatively large. It is overestimated by both MCSM and fp calculations with respective values of 182.4 and $70.9 e^2 \text{fm}^4$. This, however, is a satisfactory result considering the degree of agreement between data and calculations observed for the 2^+ and 4^+ states. The most striking feature in this respect is the small jj44 strength of $1.8 e^2 \text{fm}^4$. Furthermore, the data for the $0_2^+ \rightarrow 2_2^+$ decay mode lead to a similar observation: the $729(216) e^2 \text{fm}^4$ strength determined by the present measurement is large, and both the MCSM ($695.7 e^2 \text{fm}^4$) and the fp ($69.2 e^2 \text{fm}^4$) computations predict large strengths, while those within the jj44 space produce the smallest value of

$21.9 e^2 \text{fm}^4$. This suggests that the wave function for the 0_2^+ level is dominated by configurations within the fp space and that neutron excitations alone cannot fully account for the description of this state. This conclusion is reinforced by exploring the proton and neutron occupancies of Table VIII. It can be seen, from comparing the 0_2^+ and 2_1^+ levels, that the proton occupancies remain the same within the fp calculations. On the other hand, the MCSM result indicates a reduction of the $f_{7/2}$ orbital population for the 0_2^+ level, which appears to be redistributed into the $p_{3/2}$ and $f_{5/2}$ orbitals. In terms of the neutrons, the occupancies of these two states are, once again, similar for the fp calculations, with the main difference being a reduction in the $f_{5/2}$ occupation and a slight increase in the $p_{1/2}$ one. With regard to the MCSM computations, a significant increase in the $g_{9/2}$ occupation value up to 1.96 neutrons is computed. This is correlated with a depletion in that of both the $p_{3/2}$ and $f_{5/2}$ orbitals. Correspondingly, the jj44 calculations confirm a small $g_{9/2}$ neutron occupation. It can thus be concluded that the occupancies reinforce the observations drawn from the $B(E2)$ strengths and, as neutrons contribute with the opposite sign to the reduced transition probability, the MCSM strengths would be expected to be smaller than those of the fp calculations, as the comparison between experiment and theory indicate.

The MCSM calculations predict the largest strength with a value of $36.2 e^2 \text{fm}^4$ for the $0_3^+ \rightarrow 2_1^+$ transition, which is relatively close to the experimental value of $9.0(12) e^2 \text{fm}^4$. While the jj44 calculations are also within an order of magnitude, the fp ones are significantly underestimated. This difference with the observations for the 0_2^+ level indicates that, in this case, the $g_{9/2}$ orbital plays a larger role, which cannot be accounted for within the fp space. Moreover, it appears that both proton and neutron excitations must be included, based on the examination of the $0_3^+ \rightarrow 2_2^+$ transition strength. Here, the measured strength is large [$625_{-350}^{+250} e^2 \text{fm}^4$] and mimicked to a degree by the fp calculations ($31.9 e^2 \text{fm}^4$), whereas the jj44 and MCSM computations derive strengths smaller by an order of magnitude. From these it can be concluded that proton configurations within the fp space, as well as neutron ones, including those from the $g_{9/2}$ orbital, are involved in the 0_3^+ wave function. A further examination of the predicted orbital occupancies supports this interpretation. For the protons, the occupancy values are quite similar for both the fp and MCSM model spaces, as concluded above from the transition strengths. For the neutrons, the occupation of the $g_{9/2}$ orbital in the jj44 calculations is nearly the same as that of the 2_1^+ state, which is consistent with the observation that, in this case, the jj44 calculations perform better than the fp ones. However, the $g_{9/2}$ occupancy in the jj44 calculations is larger than that given by the MCSM ones, which could perhaps account for the fact that the MCSM computations come closest to reproducing the experimental value, i.e., a smaller $g_{9/2}$ occupation leads to a larger transition strength. Overall, the patterns observed from the transition strengths and the occupancy values for the 0_2^+ and 0_3^+ states can thus be understood in a consistent picture.

While the detailed discussion of transition strengths and orbital occupancies presented above provide an understanding

TABLE VIII. Orbital occupancy values associated with 0^+ states in ^{64}Ni , as predicted by the fp, jj44, and MCSM calculations. The occupancy values for the 2_1^+ state are included for reference. All proton occupancy values correspond to zero for the jj44 computation due to the fact that proton excitations were excluded from the model space (see text for details).

I^π	Calculation	π					ν				
		$f_{7/2}$	$p_{3/2}$	$f_{5/2}$	$p_{1/2}$	$g_{9/2}$	$f_{7/2}$	$p_{3/2}$	$f_{5/2}$	$p_{1/2}$	$g_{9/2}$
0_1^+	fp	7.51	0.37	0.1	0.03		7.92	3.22	4.03	0.83	
	jj44							3.04	3.57	0.74	0.65
	MCSM	7.35	0.40	0.1	0.03	0.10	7.84	3.14	3.58	0.82	0.58
2_1^+	fp	7.38	0.48	0.1	0.03		7.92	3.22	4.03	0.83	
	jj44							3.04	3.57	0.74	0.65
	MCSM	7.1	0.59	0.14	0.05	0.10	7.82	3.10	3.31	1.07	0.66
0_2^+	fp	7.38	0.49	0.1	0.04		7.92	3.47	3.33	1.28	
	jj44							3.56	2.58	1.5	0.35
	MCSM	5.97	1.30	0.46	0.18	0.08	7.62	2.40	2.79	1.18	1.96
0_3^+	fp	7.61	0.29	0.09	0.02		7.9	2.67	4.97	0.46	
	jj44							4.88	2.24	0.26	0.62
	MCSM	7.29	0.47	0.10	0.03	0.10	7.82	3.44	3.12	1.20	0.38

of the multistep Coulomb excitation data described in this work, it is, however, worthwhile to examine more globally the general trends exhibited by the data and to compare these with the calculations. Figures 5 and 6 provide the so-called transition networks generated from the shell-model calculations within the fp and jj44 spaces, respectively. Here the excitation energies of the calculated states are represented as dots, while the connecting lines represent the $E2$ decay paths. The widths of the various lines are directly proportional to the calculated reduced transition probabilities. Note that for each spin value, many more states than discussed thus far are presented, i.e., the plots extend up to 6–7 MeV above the yrast line.

Both interactions clearly indicate that the ground state and the 2_1^+ level are linked by a strong transition strength. This, in turn, implies that the feeding of higher spin states proceeds predominantly through multistep Coulomb excitation via the

2_1^+ level, as seen in the data. Furthermore, both calculations within the two model spaces predict that, beyond the 2_1^+ state, the excitation path splits in two directions with nearly comparable strengths and feeds the 2_2^+ and 4_2^+ states. This trend is indeed seen in the data: the measured strengths of the $2_2^+ \rightarrow 2_1^+$ and $4_2^+ \rightarrow 2_1^+$ transitions are of the same order [$2.9_{-0.2}^{+0.3}$ W.u. vs $4.5(2)$ W.u.] and only slightly lower than the $9(1)$ W.u. probability measured for the ground-state transition, as the widths in the two calculations suggest. Based on the jj44 results (see Fig. 5), the 4_1^+ state should not be observed. In this instance, the data favor the fp model space, as the $4_1^+ \rightarrow 2_1^+$ strength has been determined experimentally and found to be smaller than that linking the 4_1^+ and 2_2^+ states, in qualitative agreement with the calculations in this space. In fact, the similarity between the data and the fp calculations extends clearly to the 0_2^+ level, where the computed deexcitation pattern also

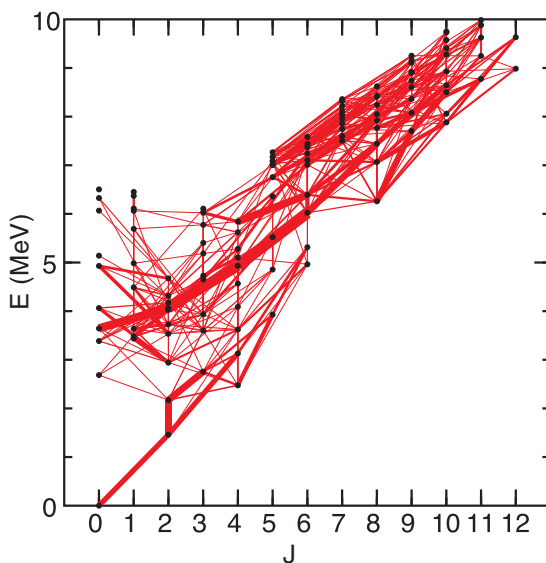


FIG. 5. Plot of the reduced transition strengths connecting states in ^{64}Ni , as predicted by the jj44 calculations (see text for details).

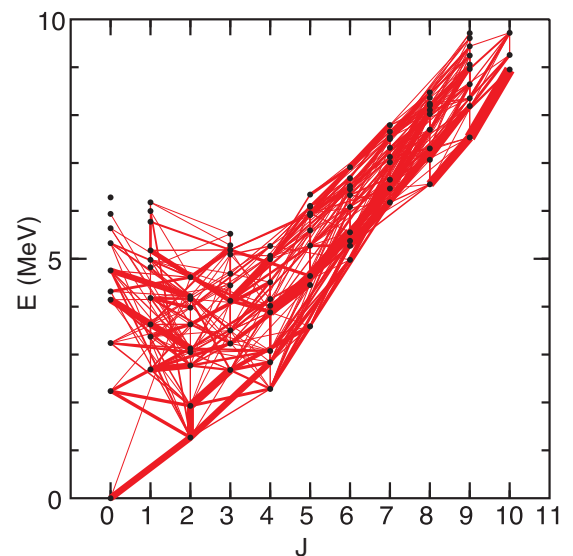


FIG. 6. Plot of the reduced transition strengths connecting states in ^{64}Ni , as predicted by the fp calculations (see text for details).

mirrors that seen in the measurements. Specifically, the noted absence of a $0_2^+ \rightarrow 2_1^+$ transition in the jj44 prediction is not supported by the data. Indeed, the fact that all the transitions out of the 0_2^+ state in Fig. 6 are of comparable width, i.e., of the same order of magnitude, can be viewed as a signature for a small degree of collectivity. This observation agrees with the results of the MCSM calculations that associate the 0_2^+ state with a small, oblate deformation.

In Figs. 5 and 6, signatures of strong collectivity are manifest through the appearance of sequences with the same strength linking successive states separated by two units of angular momentum. While no such band is present in the shell-model calculations within the fp space, one is clearly visible within the jj44 computation (Fig. 5). Indeed, a rather clear $8^+ - 6^+ - 4^+ - 2^+ - 0^+$ sequence appears, terminating in the calculated 0_4^+ level at an excitation energy of 3.646 MeV. Assuming that the jj44 calculations are a close representation of the data, the question then arises as to why this 0_4^+ state, and by extension, the cascade of collective $E2$ transitions built on it was not observed in the present investigation. As indicated in Fig. 5, the strengths of transitions linking the states in the cascade with the lower-lying, near yrast states are small. In terms of multistep Coulomb excitation, this implies that the cross section for populating the 0_4^+ state must be small as well and that, hence, the associated transitions such as the $0_4^+ \rightarrow 2_2^+$ link would be below the detection limit of the experiment. It is also worth noting that the entire band in Fig. 5 is not calculated to become yrast, even at spin 10 or above. This would also account for the fact that such a collective sequence was not observed in measurements following deep-inelastic reactions with the $^{64}\text{Ni} + ^{238}\text{U}$ [36] and $^{26}\text{Mg} + ^{48}\text{Ca}$ [51] systems.

C. Evidence for a 0_4^+ state

From the discussion above and the calculations illustrated in Figs. 5 and 6, it is clear that observing a 0_4^+ state through multistep Coulomb excitation would be very challenging, if not impossible. Nevertheless, the decay patterns delineated in Fig. 5 as well as the results of similar calculations within the MCSM framework (not shown) stimulated further attempts to identify possible candidates for a 0^+ level associated with a prolate minimum. Following a neutron capture measurement [36], a 0_4^+ state at 3463 keV which decays in part via a 1187-keV transition to the 2_2^+ , 2277-keV level was observed. As expected, the $0_4^+ \rightarrow 2_2^+$ transition was not observed in the present Coulomb excitation data. However, an upper limit of $1.3 e^2 \text{fm}^4$ or 0.08 W.u. was established for the $B(E2; 0_4^+ \rightarrow 2_2^+)$ transition strength from the spectra at backward angles. With this value, the similarity between the low-spin structures of ^{66}Ni and ^{64}Ni is striking. Indeed, both nuclei reveal the presence of three excited 0^+ states with similar deexcitation patterns. Specifically, the 0_2^+ levels in both ^{66}Ni and ^{64}Ni decay toward the respective 2_1^+ states with strengths of 4.3 W.u. and 3.2(2) W.u., while the 0_3^+ states have corresponding $B(E2)$ values of 0.1 and 0.59(8) W.u., respectively. Likewise, the 0.2 W.u. value reported for the 0_4^+ state in ^{66}Ni compares with the 0.08 W.u. upper limit reported here for ^{64}Ni . In view of these observations and based on the results of the MCSM

calculations, it is concluded that the 0_1^+ and 0_3^+ levels are associated with a spherical shape, the 0_2^+ state with an oblate one, and the 0_4^+ state with a prolate shape. As predicted by these calculations, the excitation energy of the three modes increases with decreasing neutron number: the measured 0_2^+ energy increases from 2443 to 2867 keV between ^{66}Ni and ^{64}Ni , that of the 0_3^+ levels increases from 2671 to 3026 keV, and the 0_4^+ states are located at 2974 and 3463 keV, respectively. Hence, the structure of ^{64}Ni is understood in terms of shape coexistence based on the available experimental evidence. The reader is referred to the work of Ref. [36] for an in-depth discussion.

V. CONCLUSIONS

The electromagnetic properties of low-lying states and the possible presence of shape coexisting states in ^{64}Ni were investigated following a multistep Coulomb excitation measurement. The experiment was performed at the ATLAS accelerator facility using the γ -ray tracking array, GRETINA, in conjunction with the CHICO2 particle detector. Transition and diagonal matrix elements were extracted from the measured γ -ray yields using GOSIA, a semiclassical coupled-channel analysis code. Reduced transition probabilities and spectroscopic quadrupole moments deduced from the matrix elements were compared with those predicted by conventional shell-model calculations with the jj44 and fp effective interactions as well as those within the Monte Carlo shell-model (MCSM) framework. Transition strengths for the deexcitation of the known excited 0^+ states were found to be reproduced well by theory and, in general, supported the view that the nucleus, ^{64}Ni , closely resembles its neighbor ^{66}Ni , herewith favoring an interpretation in terms of shape coexistence. In particular, transition strengths and quadrupole moments indicate that the ground and 0_3^+ states are spherical, and the 0_2^+ level is characterized by a small oblate deformation. In addition, the convergence between the experimentally deduced $B(E2)$ strengths and the calculated ones indicates that most excitations observed in the present data are confined to the fp shell. Furthermore, while more study is necessary in order to further assess the nature of these states, the agreement between experiment and theory, alongside the trends seen in the Ni chain, make a strong case for shape coexistence in this nucleus.

ACKNOWLEDGMENTS

The authors gratefully acknowledge help with the experiment from K. Auranen, C. M. Campbell, H. L. Crawford, A. B. Hayes, D. Cline, and Krishichayan. This material is based upon work supported by the U.S. Department of Energy, Office of Science, Office of Nuclear Physics, under Grants No. DE-FG02-97ER41041 (UNC), No. DE-FG02-97ER41033 (TUNL), No. DE-FG02-08ER41556 and No. DE-SC0020451 (MSU), No. DE-FG02-94ER40848 (UML), No. DE-FG02-94ER4084 (Maryland), and Contracts No. DE-AC02-06CH11357 (ANL), No. DE-AC52-07NA27344 (LLNL), No. DE-AC02-05CH11231 (LBNL), No. DE-SC0020451 (MSU), by the National Science Foundation

under Grants No. PHY-1565546 (MSU), and by the UNC Startup Funds of ADA. The MCSM calculations were performed on the K computer at RIKEN AICS and Oakforest-PACS operated by JCAHPC (hp160211, hp170230, hp180179, hp190160, hp200130). This work was supported in part by MEXT as “Priority Issue on Post-K Computer”

(Elucidation of the Fundamental Laws and Evolution of the Universe) and “Program for Promoting Research on the Super-Computer Fugaku” (Simulation for Basic Science: From Fundamental Laws of Particles to Creation of Nuclei), and by JICFuS. This research used resources of ANLs ATLAS Facility, which is a DOE Office of Science User Facility.

- [1] M. Pomorski, M. Pfützner, W. Dominik, R. Grzywacz, A. Stolz, T. Baumann, J. S. Berryman, H. Czyrkowski, R. Dabrowski, A. Fijałkowska, T. Ginter, J. Johnson, G. Kamiński, N. Larson, S. N. Liddick, M. Madurga, C. Mazzocchi, S. Mianowski, K. Miernik, D. Miller *et al.*, *Phys. Rev. C* **90**, 014311 (2014).
- [2] R. Taniuchi, C. Santamaria, P. Doornenbal, A. Obertelli, K. Yoneda, G. Authelet, H. Baba, D. Calvet, F. Château, A. Corsi, A. Delbart, J. M. Gheller, A. Gillibert, J. D. Holt, T. Isobe, V. Lapoux, M. Matsushita, J. Menéndez, S. Momiyama, T. Motobayashi *et al.*, *Nature (London)* **569**, 53 (2019).
- [3] M. Bernas, P. Dessagne, M. Langevin, J. Payet, F. Pougheon, and P. Roussel, *Phys. Lett. B* **113**, 279 (1982).
- [4] R. Broda, B. Fornal, W. Królas, T. Pawłat, D. Bazzacco, S. Lunardi, C. Rossi-Alvarez, R. Menegazzo, G. de Angelis, P. Bednarczyk, J. Rico, D. De Acuña, P. J. Daly, R. H. Mayer, M. Sferrazza, H. Grawe, K. H. Maier, and R. Schubart, *Phys. Rev. Lett.* **74**, 868 (1995).
- [5] S. Suchyta, S. N. Liddick, Y. Tsunoda, T. Otsuka, M. B. Bennett, A. Chemey, M. Honma, N. Larson, C. J. Prokop, S. J. Quinn, N. Shimizu, A. Simon, A. Spyrou, V. Tripathi, Y. Utsuno, and J. M. VonMoss, *Phys. Rev. C* **89**, 021301(R) (2014).
- [6] B. Crider, C. Prokop, S. Liddick, M. Al-Shudifat, A. Ayangeakaa, M. Carpenter, J. Carroll, J. Chen, C. Chiara, H. David, A. Dombos, S. Go, R. Grzywacz, J. Harker, R. Janssens, N. Larson, T. Lauritsen, R. Lewis, S. Quinn, F. Recchia *et al.*, *Phys. Lett. B* **763**, 108 (2016).
- [7] A. I. Morales, G. Benzoni, H. Watanabe, S. Nishimura, F. Browne, R. Daido, P. Doornenbal, Y. Fang, G. Lorusso, Z. Patel, S. Rice, L. Sinclair, P.-A. Söderström, T. Sumikama, J. Wu, Z. Y. Xu, A. Yagi, R. Yokoyama, H. Baba, R. Avigo *et al.*, *Phys. Rev. C* **93**, 034328 (2016).
- [8] S. Leoni, B. Fornal, N. Mărginean, M. Sferrazza, Y. Tsunoda, T. Otsuka, G. Bocchi, F. C. L. Crespi, A. Bracco, S. Aydin, M. Boromiza, D. Bucurescu, N. Cieplicka-Oryczak, C. Costache, S. Călinescu, N. Florea, D. G. Ghiță, T. Glodariu, A. Ionescu, L. W. Iskra *et al.*, *Phys. Rev. Lett.* **118**, 162502 (2017).
- [9] B. Olaizola, L. M. Fraile, H. Mach, A. Poves, F. Nowacki, A. Aprahamian, J. A. Briz, J. Cal-González, D. Ghița, U. Köster, W. Kurcewicz, S. R. Lesher, D. Pauwels, E. Picado, D. Radulov, G. S. Simpson, and J. M. Udías, *Phys. Rev. C* **95**, 061303(R) (2017).
- [10] T. Otsuka, T. Suzuki, R. Fujimoto, H. Grawe, and Y. Akaishi, *Phys. Rev. Lett.* **95**, 232502 (2005).
- [11] T. Otsuka and Y. Tsunoda, *J. Phys. G: Nucl. Part. Phys.* **43**, 024009 (2016).
- [12] Y. Tsunoda, T. Otsuka, N. Shimizu, M. Honma, and Y. Utsuno, *Phys. Rev. C* **89**, 031301(R) (2014).
- [13] S. N. Liddick, W. B. Walters, C. J. Chiara, R. V. F. Janssens, B. Abromeit, A. Ayres, A. Bey, C. R. Bingham, M. P. Carpenter, L. Cartegni, J. Chen, H. L. Crawford, I. G. Darby, R. Grzywacz, J. Harker, C. R. Hoffman, S. Ilyushkin, F. G. Kondev, N. Larson, M. Madurga *et al.*, *Phys. Rev. C* **92**, 024319 (2015).
- [14] S. N. Liddick, W. B. Walters, C. J. Chiara, R. V. F. Janssens, B. Abromeit, A. Ayres, A. Bey, C. R. Bingham, M. P. Carpenter, L. Cartegni, J. Chen, H. L. Crawford, I. G. Darby, R. Grzywacz, J. Harker, C. R. Hoffman, S. Ilyushkin, F. G. Kondev, N. Larson, M. Madurga *et al.*, *Phys. Rev. C* **94**, 069904(E) (2016).
- [15] A. Gade, R. V. F. Janssens, T. Baugher, D. Bazin, B. A. Brown, M. P. Carpenter, C. J. Chiara, A. N. Deacon, S. J. Freeman, G. F. Grinyer, C. R. Hoffman, B. P. Kay, F. G. Kondev, T. Lauritsen, S. McDaniel, K. Meierbachtol, A. Ratkiewicz, S. R. Stroberg, K. A. Walsh, D. Weisshaar *et al.*, *Phys. Rev. C* **81**, 051304(R) (2010).
- [16] P. Adrich, A. M. Amthor, D. Bazin, M. D. Bowen, B. A. Brown, C. M. Campbell, J. M. Cook, A. Gade, D. Galaviz, T. Glasmacher, S. McDaniel, D. Miller, A. Obertelli, Y. Shimbara, K. P. Siwek, J. A. Tostevin, and D. Weisshaar, *Phys. Rev. C* **77**, 054306 (2008).
- [17] S. N. Liddick, S. Suchyta, B. Abromeit, A. Ayres, A. Bey, C. R. Bingham, M. Bolla, M. P. Carpenter, L. Cartegni, C. J. Chiara, H. L. Crawford, I. G. Darby, R. Grzywacz, G. Gürdal, S. Ilyushkin, N. Larson, M. Madurga, E. A. McCutchan, D. Miller, S. Padgett *et al.*, *Phys. Rev. C* **84**, 061305(R) (2011).
- [18] J. M. Dugas, I. Matea, J.-P. Delaroche, M. Pfützner, M. Sawicka, F. Becker, G. Bélier, C. R. Bingham, R. Borcea, E. Bouchez, A. Buta, E. Dragulescu, G. Georgiev, J. Giovinazzo, M. Girod, H. Grawe, R. Grzywacz, F. Hammache, F. Ibrahim, M. Lewitowicz *et al.*, *Phys. Rev. C* **83**, 054312 (2011).
- [19] D. Pauwels, O. Ivanov, N. Bree, J. Büscher, T. E. Cocolios, J. Gentens, M. Huyse, A. Korgul, Y. Kudryavtsev, R. Raabe, M. Sawicka, I. Stefanescu, J. Van de Walle, P. Van den Bergh, P. Van Duppen, and W. B. Walters, *Phys. Rev. C* **78**, 041307(R) (2008).
- [20] N. Hoteling, C. J. Chiara, R. Broda, W. B. Walters, R. V. F. Janssens, M. Hjorth-Jensen, M. P. Carpenter, B. Fornal, A. A. Hecht, W. Królas, T. Lauritsen, T. Pawłat, D. Seweryniak, X. Wang, A. Wöhr, J. Wrzesiński, and S. Zhu, *Phys. Rev. C* **82**, 044305 (2010).
- [21] A. Deacon, S. Freeman, R. Janssens, F. Xu, M. Carpenter, I. Calderin, P. Chowdhury, N. Hammond, T. Lauritsen, C. Lister, D. Seweryniak, J. Smith, S. Tabor, B. Varley, and S. Zhu, *Phys. Lett. B* **622**, 151 (2005).
- [22] S. Zhu, A. N. Deacon, S. J. Freeman, R. V. F. Janssens, B. Fornal, M. Honma, F. R. Xu, R. Broda, I. R. Calderin, M. P. Carpenter, P. Chowdhury, F. G. Kondev, W. Królas, T. Lauritsen, S. N. Liddick, C. J. Lister, P. F. Mantica, T. Pawłat, D. Seweryniak, J. F. Smith *et al.*, *Phys. Rev. C* **74**, 064315 (2006).
- [23] N. Hoteling, W. B. Walters, R. V. F. Janssens, R. Broda, M. P. Carpenter, B. Fornal, A. A. Hecht, M. Hjorth-Jensen, W. Królas, T. Lauritsen, T. Pawłat, D. Seweryniak, X. Wang, A. Wöhr, J. Wrzesiński, and S. Zhu, *Phys. Rev. C* **74**, 064313 (2006).
- [24] A. N. Deacon, S. J. Freeman, R. V. F. Janssens, M. Honma, M. P. Carpenter, P. Chowdhury, T. Lauritsen, C. J. Lister, D. Seweryniak, J. F. Smith, S. L. Tabor, B. J. Varley, F. R. Xu, and S. Zhu, *Phys. Rev. C* **76**, 054303 (2007).

- [25] M. P. Carpenter, R. V. F. Janssens, and S. Zhu, *Phys. Rev. C* **87**, 041305(R) (2013).
- [26] G. Benzoni, A. Morales, H. Watanabe, S. Nishimura, L. Coraggio, N. Itaco, A. Gargano, F. Browne, R. Daido, P. Doornenbal, Y. Fang, G. Lorusso, Z. Patel, S. Rice, L. Sinclair, P.-A. Söderström, T. Sumikama, J. Wu, Z. Xu, R. Yokoyama *et al.*, *Phys. Lett. B* **751**, 107 (2015).
- [27] A. D. Ayangeakaa, S. Zhu, R. V. F. Janssens, M. P. Carpenter, M. Albers, M. Alcorta, T. Baugher, P. F. Bertone, C. J. Chiara, P. Chowdhury, H. M. David, A. N. Deacon, B. DiGiovine, A. Gade, C. R. Hoffman, F. G. Kondev, T. Lauritsen, C. J. Lister, E. A. McCutchan, D. S. Moerland *et al.*, *Phys. Rev. C* **91**, 044327 (2015).
- [28] C. Santamaria, C. Louchart, A. Obertelli, V. Werner, P. Doornenbal, F. Nowacki, G. Authelet, H. Baba, D. Calvet, F. Château, A. Corsi, A. Delbart, J.-M. Gheller, A. Gillibert, T. Isobe, V. Lapoux, M. Matsushita, S. Momiyama, T. Motobayashi, M. Niikura *et al.*, *Phys. Rev. Lett.* **115**, 192501 (2015).
- [29] A. Gade, R. V. F. Janssens, D. Bazin, P. Farris, A. M. Hill, S. M. Lenzi, J. Li, D. Little, B. Longfellow, F. Nowacki, A. Poves, D. Rhodes, J. A. Tostevin, and D. Weisshaar, *Phys. Rev. C* **103**, 014314 (2021).
- [30] A. Gade, R. V. F. Janssens, B. A. Brown, R. G. T. Zegers, D. Bazin, P. Farris, A. M. Hill, J. Li, D. Little, B. Longfellow, F. Nowacki, D. Rhodes, and D. Weisshaar, *Phys. Rev. C* **104**, 024313 (2021).
- [31] N. Sensharma, A. D. Ayangeakaa, R. V. F. Janssens, Q. B. Chen, S. Zhu, M. Alcorta, M. P. Carpenter, E. A. McCutchan, F. G. Kondev, T. Lauritsen, D. Seweryniak, C. R. Hoffman, A. M. Rogers, A. Gade, T. Baugher, and P. Chowdhury, *Phys. Rev. C* **105**, 044315 (2022).
- [32] M. Albers, S. Zhu, R. V. F. Janssens, J. Gellanki, I. Ragnarsson, M. Alcorta, T. Baugher, P. F. Bertone, M. P. Carpenter, C. J. Chiara, P. Chowdhury, A. N. Deacon, A. Gade, B. DiGiovine, C. R. Hoffman, F. G. Kondev, T. Lauritsen, C. J. Lister, E. A. McCutchan, D. S. Moerland *et al.*, *Phys. Rev. C* **88**, 054314 (2013).
- [33] M. Albers, S. Zhu, A. D. Ayangeakaa, R. V. F. Janssens, J. Gellanki, I. Ragnarsson, M. Alcorta, T. Baugher, P. F. Bertone, M. P. Carpenter, C. J. Chiara, P. Chowdhury, H. M. David, A. N. Deacon, B. DiGiovine, A. Gade, C. R. Hoffman, F. G. Kondev, T. Lauritsen, C. J. Lister *et al.*, *Phys. Rev. C* **94**, 034301 (2016).
- [34] R. Broda, T. Pawlat, W. Królas, R. V. F. Janssens, S. Zhu, W. B. Walters, B. Fornal, C. J. Chiara, M. P. Carpenter, N. Hoteling, L. W. Iskra, F. G. Kondev, T. Lauritsen, D. Seweryniak, I. Stefanescu, X. Wang, and J. Wrzesiński, *Phys. Rev. C* **86**, 064312 (2012).
- [35] S. Zhu, R. V. F. Janssens, M. P. Carpenter, C. J. Chiara, R. Broda, B. Fornal, N. Hoteling, W. Królas, T. Lauritsen, T. Pawlat, D. Seweryniak, I. Stefanescu, J. R. Stone, W. B. Walters, X. Wang, and J. Wrzesiński, *Phys. Rev. C* **85**, 034336 (2012).
- [36] N. Märginean, D. Little, Y. Tsunoda, S. Leoni, R. V. F. Janssens, B. Fornal, T. Otsuka, C. Michelagnoli, L. Stan, F. C. L. Crespi, C. Costache, R. Lica, M. Sferrazza, A. Turturica, A. D. Ayangeakaa, K. Auranen, M. Barani, P. C. Bender, S. Bottoni, M. Boromiza *et al.*, *Phys. Rev. Lett.* **125**, 102502 (2020).
- [37] S. Paschalis, I. Y. Lee, A. O. Macchiavelli, C. M. Campbell, M. Cromaz, S. Gros, J. Pavan, J. Qian, R. M. Clark, H. L. Crawford, D. Doering, P. Fallon, C. Lionberger, T. Loew, M. Petri, T. Stezelberger, S. Zimmermann, D. C. Radford, K. Lagergren, D. Weisshaar, R. Winkler, T. Glasmacher, J. T. Anderson, and C. W. Beausang, *Nucl. Instrum. Methods Phys. Res. Sect. A* **709**, 44 (2013).
- [38] C. Y. Wu, D. Cline, A. Hayes, R. S. Flight, A. M. Melchionna, C. Zhou, I. Y. Lee, D. Swan, R. Fox, and J. T. Anderson, *Nucl. Instrum. Methods Phys. Res. Sect. A* **814**, 6 (2016).
- [39] B. Singh and J. Chen, *Nucl. Data Sheets* **178**, 41 (2021).
- [40] T. Czosnyka, D. Cline, and C. Y. Wu, *Bull. Am. Phys. Soc.* **28**, 745 (1983).
- [41] J. M. Allmond, B. A. Brown, A. E. Stuchbery, A. Galindo-Uribarri, E. Padilla-Rodal, D. C. Radford, J. C. Batchelder, M. E. Howard, J. F. Liang, B. Manning, R. L. Varner, and C.-H. Yu, *Phys. Rev. C* **90**, 034309 (2014).
- [42] O. Kenn, K.-H. Speidel, R. Ernst, J. Gerber, P. Maier-Komor, and F. Nowacki, *Phys. Rev. C* **63**, 064306 (2001).
- [43] A. F. Lisetskiy, B. A. Brown, M. Horoi, and H. Grawe, *Phys. Rev. C* **70**, 044314 (2004).
- [44] M. Honma, T. Otsuka, B. A. Brown, and T. Mizusaki, *Eur. Phys. J. A* **25**, 499 (2005).
- [45] D. Steppenbeck, S. Takeuchi, N. Aoi, P. Doornenbal, M. Matsushita, H. Wang, H. Baba, N. Fukuda, S. Go, M. Honma, J. Lee, K. Matsui, S. Michimasa, T. Motobayashi, D. Nishimura, T. Otsuka, H. Sakurai, Y. Shiga, P. A. Söderström, T. Sumikama *et al.*, *Nature (London)* **502**, 207 (2013).
- [46] R. V. F. Janssens, B. Fornal, P. F. Mantica, B. A. Brown, R. Broda, P. Bhattacharyya, M. P. Carpenter, M. Cinausero, P. J. Daly, A. D. Davies, T. Glasmacher, Z. W. Grabowski, D. E. Groh, M. Honma, F. G. Kondev, W. Królas, T. Lauritsen, S. N. Liddick, S. Lunardi, N. Marginean *et al.*, *Phys. Lett. B* **546**, 55 (2002).
- [47] J. Prisciandaro, P. Mantica, B. Brown, D. Anthony, M. Cooper, A. Garcia, D. Groh, A. Komives, W. Kumarasiri, P. Lofy, A. Oros-Peusquens, S. Tabor, and M. Wiedeking, *Phys. Lett. B* **510**, 17 (2001).
- [48] T. Otsuka, M. Honma, T. Mizusaki, N. Shimizu, and Y. Utsuno, *Prog. Part. Nucl. Phys.* **47**, 319 (2001).
- [49] N. Shimizu, Y. Utsuno, T. Mizusaki, M. Honma, Y. Tsunoda, and T. Otsuka, *Phys. Rev. C* **85**, 054301 (2012).
- [50] F. G. Kondev (private communication).
- [51] D. Little, Ph.D. thesis, University of North Carolina at Chapel Hill, 2020.